

Introduction of a Symmetric Tight Wavelet Frame to Image Fusion Methods Based on Substitutive Wavelet Decomposition

Myungjin Choi

Abstract—A useful technique in various applications of remote sensing involves the fusion of panchromatic and multispectral images. Wavelet-based approaches to image fusion generally produce high-quality spectral content in fused images. However, the spatial resolution obtained by most wavelet-based methods is less than that obtained by the intensity-hue-saturation (IHS) method. Recent studies show that if an undecimated discrete wavelet transform (DWT) is used for image fusion, the spatial resolution of the fused images can be as good as that of images obtained by the IHS method. This effect occurs because an undecimated DWT is exactly shift-invariant. In this paper, the author introduces a symmetric tight wavelet frame to image fusion methods that are based on substitutive wavelet decomposition. The introduced tight wavelet frame transform is nearly shift-invariant with desired properties such as wavelet smoothness, short support, and symmetry. The experimental results show the possibility as an alternative DWT approach for image fusion. In addition, the author proposes a fast algorithm for an improved IHS method introduced by González-Audícana et al. The proposed approach enables a fast, easy, and extendable implementation. Hence, for the fusion of IKONOS panchromatic and multispectral images, the near-infrared band of IKONOS may be included in the definition of the intensity component. This approach produces satisfactory results, both visually and quantitatively.

Index Terms—Image fusion, intensity-hue-saturation transform, multiresolution analysis, tight wavelet frame, IKONOS image, wavelet transform.

I. INTRODUCTION

THE TECHNIQUE of fusing a panchromatic (Pan) image that has a high-spatial and low-spectral resolution with multispectral (MS) images that have a low-spatial and high-spectral resolution is very useful in many remote sensing applications that require both high-spatial and high-spectral resolution, especially for GIS-based applications.

An image that has been well fused by an effective fusion technique is useful for not only increasing the capability of humans to interpret the image but also improving the accuracy of the classification [1]. Moreover, a well-fused image gives a visually beautiful color image, especially for visualization purposes [2].

Many image fusion techniques and software tools have been developed for specific applications. Of the hundreds of

image fusion techniques, the best known are the intensity-hue-saturation (IHS) method, principal component analysis, arithmetic combinations, and wavelet-based fusion methods [2].

Wavelet-based fusion methods, in particular, which are widely used to fuse images, are based on multiresolution analysis. The wavelet approach preserves the spectral characteristics of MS images better than the IHS method. In general, however, images fused by wavelet-based methods have much less spatial information than images fused by the IHS method. Nonetheless, recent studies have shown that if an undecimated discrete wavelet transform (DWT) is used instead of the critically sampled DWT, the spatial resolution of fused images can be as good as the resolution of images fused with the IHS method. An undecimated DWT, which is a shift-invariant form of the DWT, can be implemented by removing the down-sampling operations in the usual DWT implementation. Undecimated DWTs can thereby avoid some of the artifacts that arise when a critically sampled DWT is used for image fusion [3]–[9].

Researchers have recently discussed and analyzed the theory of frames and oversampled filterbanks [10]–[17]. As is well known, the critically sampled DWT does not allow for symmetry, except for the Haar wavelet. In addition, because of the critical sampling, orthogonal filters suffer from a pronounced lack of shift invariance. The desirable properties can be achieved through the design of tight frame filterbanks, of which orthogonal filters are a special case. In contrast to orthogonal filters, tight frame filters have a redundancy that allows for an approximate shift invariance due to the dense plane of the time scale. Tight frame filterbanks are also shorter and result in smoother scaling and wavelet functions, in addition to producing symmetry [17]. In the next chapter, the design of a three-band symmetric tight frame filterbank will be introduced.

Wavelet-based fusion methods are not efficient enough to quickly merge massive volumes of data from new satellite images because of their high computational complexity. Hence, an advanced fusion scheme is needed, particularly a scheme with a fast computing capability and one which can obtain a high spatial quality and preserve spectral information. The author therefore introduces a fast algorithm for the substitutive wavelet on the intensity (SWI) method that was recently introduced by González-Audícana et al. [7]. In the SWI method, multiresolution wavelet decomposition is used to execute the detailed extraction phase, and the IHS transform is followed

This work was supported by Korea Research Foundation Grant (D00190) and in part by the Research Program of Satellite Technology Research Center, Korea Advanced Institute of Science and Technology.

M.-J. Choi is with Satellite Technology Research Center, Korea Advanced Institute of Science and Technology, 373-1, Guseong-dong, Yuseong-gu, Daejeon, 305-701, Korea (email:prime@satrec.kaist.ac.kr).

to inject the spatial detail of a Pan image into an MS image. This approach performs significantly better than other wavelet-based methods [7], [9].

One disadvantage of fusion methods that are based on the IHS transform is that they can only be applied to three-band RGB compositions. Therefore, the fast IHS method (FIHS) introduced by Tu et al. [18] was considered in this paper. Aside from its fast computing capability for fusing images, this method can extend traditional three-order transformations to an arbitrary order. In addition, in the SWI method, Gonzalez-Audicana et al. applied the wavelet transform to both the intensity image and the Pan image and then performed an inverse wavelet transform to a set composed of the low-frequency version (or the smoothed plane) of the wavelet-transformed intensity image and the sum of the high-frequency versions (or the sum of wavelet planes) of the wavelet-transformed Pan image. This is to add the spatial detail information of the Pan image into the intensity image. To simplify this procedure, a wavelet transform was used to directly extract detailed information from the difference image of the Pan image and the intensity image. As a result, we could easily obtain fused images with the fast scheme of the SWI method; We simply added the detailed information extracted from the difference image of the Pan image and the intensity image to each MS image. The fast SWI (FSWI) scheme is much simpler and faster than the SWI method. Moreover, the FSWI scheme is theoretically the same as the SWI method.

In contrast, the most popular wavelet transforms for image fusion are Mallat's algorithm and the *à trous* algorithm. Mallat's algorithm is an orthogonal, decimated, nonredundant DWT algorithm, but it is nonsymmetric (except for the Haar wavelet) and non-shift-invariant. The *à trous* algorithm is a symmetric, shift-invariant DWT algorithm, but it is non-orthogonal, undecimated and redundant. The author therefore introduce, as an alternative approach to the two popular DWTs, a symmetric, nearly shift-invariant, decimated DWT algorithm that is nonorthogonal and redundant (though only about twice as redundant as Mallat's algorithm). We call the critically sampled Mallat's algorithm the DWT [19]; the undecimated *à trous* DWT the ADWT [20]; and the introduced twice-redundant DWT the 2XDWT [21].

To verify the 2XDWT for image fusion, the fusion of an IKONOS Pan image and an MS image was considered. In addition, the spatial and spectral quality of the resulting images with the five estimators was analyzed.

II. THE CONSTRUCTION OF A SYMMETRIC TIGHT WAVELET FRAME BASED ON A THREE-BAND FILTERBANK

As is well known, except for the Haar filterbank, two-band finite impulse response (FIR) orthogonal filterbanks do not allow for symmetry. In addition, the imposition of orthogonality for the two-band FIR filterbanks requires relatively long filter support for such properties as a high level of smoothness in the resulting scaling function and wavelets, as well as a high approximation order. Symmetry and orthogonality can both be obtained if the filterbanks have more than two bands (see [22]

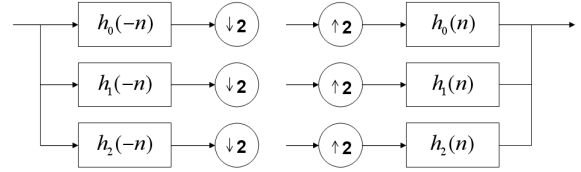


Fig. 1. A three-band perfect reconstruction filterbank

for more details). Furthermore, due to the critical sampling, orthogonal filters suffer from a pronounced lack of shift invariance, though the desirable properties can be achieved through the design of tight frame filterbanks, of which orthogonal filters are a special case. In contrast to orthogonal filters, tight frame filters have a level of redundancy that allows for the approximate shift invariance behavior caused by the dense time-scale plane. Besides producing symmetry, tight frame filterbanks are shorter and result in smoother scaling and wavelet functions. For more information on the basic concepts of frame theory and oversampled filterbanks, refer to references [10]–[17]. In this section, the construction of a symmetric tight wavelet frame based on a three-band tight frame filterbank will be briefly introduced (see [21] and [23] for more details). The results and an example will be also provided.

A. A Symmetric Tight Wavelet Frame with Two Generators

1) *PR Conditions and Symmetry Condition:* The PR conditions for the three-band filterbank, which are illustrated in Fig. 1, can be obtained by the following two equations:

$$\sum_{i=0}^2 H_i(z)H_i(z^{-1}) = 2 \quad (1)$$

$$\sum_{i=0}^2 H_i(-z)H_i(z^{-1}) = 0 \quad (2)$$

The PR conditions can also be written in matrix form as

$$H^T(z)H(z^{-1}) = I, \quad (3)$$

where

$$H(z) = \begin{pmatrix} H_0(z) & H_0(-z) \\ H_1(z) & H_1(-z) \\ H_2(z) & H_2(-z) \end{pmatrix}.$$

Also, if $h_0(n)$ is compactly supported, then a solution $\{h_1(n), h_2(n)\}$ to Eq.(3) exists if and only if

$$|H_0(z)|^2 + |H_0(-z)|^2 < 2, \quad |z| = 1. \quad (4)$$

A wavelet tight frame with only two symmetric or antisymmetric wavelets is generally impossible to obtain with a compactly supported symmetric scaling function, $\phi(t)$. However, Petukhov states a condition that the lowpass filter $h_0(n)$ must satisfy so that this becomes possible [24]. Therefore, if $h_0(n)$ is symmetric, compactly supported, and satisfies Eq.(4), then an (anti)symmetric solution $\{h_1(n), h_2(n)\}$ to Eq.(3) exists if and only if all the roots of

$$2 - H_0(z)H_0(z^{-1}) + H_0(-z)H_0(-z^{-1}) \quad (5)$$

have even multiplicity.

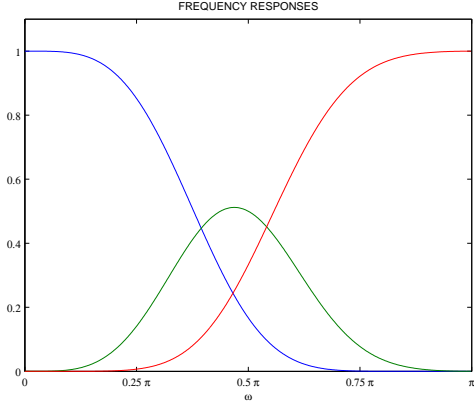


Fig. 2. The frequency responses of h_0 , h_1 , and h_2 in the example

2) *Case* $H_2(z) = H_1(-z)$: The goal is to design a set of three filters that satisfy the PR conditions in which the lowpass filter, $h_0(n)$, is symmetric and the filters $h_1(n)$ and $h_2(n)$ are each either symmetric or antisymmetric. There are two cases. Case I denotes the case where $h_1(n)$ is symmetric and $h_2(n)$ is antisymmetric. Case II denotes the case where $h_1(n)$ and $h_2(n)$ are both antisymmetric. The symmetry condition for $h_0(n)$ is

$$h_0(n) = h_0(N - 1 - n), \quad (6)$$

where N is the length of the filter $h_0(n)$.

We dealt only with Case I of even-length filters. Solutions for Case I can be obtained from solutions where $h_2(n)$ is a time-reversed version of $h_1(n)$ (and where neither filter is (anti)symmetric).

To show this, suppose that $h_0(n)$, $h_1(n)$, and $h_2(n)$ satisfy the PR conditions and that

$$h_2(n) = h_1(N - 1 - n). \quad (7)$$

Then, by defining

$$h_1^{new} = \frac{1}{\sqrt{2}}(h_1(n) + h_2(n - 2d)), \quad (8)$$

$$h_2^{new} = \frac{1}{\sqrt{2}}(h_1(n) - h_2(n - 2d)) \text{ with } d \in \mathbb{Z}, \quad (9)$$

the filters h_0 , h_1^{new} , and h_2^{new} also satisfy the PR conditions, and h_1^{new} and h_2^{new} are symmetric and antisymmetric as follows:

$$\begin{aligned} h_1^{new}(n) &= h_1^{new}(N_2 - 1 - n), \\ h_2^{new}(n) &= -h_2^{new}(N_2 - 1 - n), \end{aligned}$$

where $N_2 = N + 2d$.

We state main results of the paper [21] without the proof. The filters $h_0(n)$, $h_1(n)$, and $h_2(n)$ with symmetries in Eq.(6) and Eq.(7) satisfy the PR conditions if polyphase components of the filters are given by

$$H_{0,0}(z) = z^{-M/2} \sqrt{2} A(z) B(z^{-1}), \quad (10)$$

$$H_{1,0}(z) = A^2(z), \quad (11)$$

$$H_{1,1}(z) = -B^2(z), \quad (12)$$

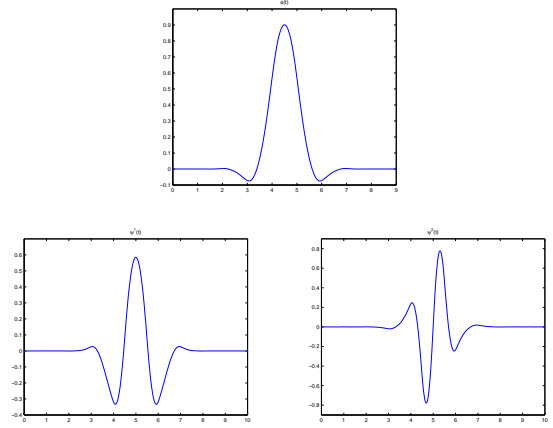


Fig. 3. The symmetric scaling function, $\phi(t)$, and the two wavelets $\psi^1(t)$ and $\psi^2(t)$ of the example

TABLE I
COEFFICIENTS FOR THE EXAMPLE

n	$h_0(n)$	$h_1(n)$	$h_2(n)$
0	0.00069616789827	-0.00014203017443	0.00014203017443
1	-0.02692519074183	0.00549320005590	-0.00549320005590
2	-0.04145457368920	0.01098019299363	-0.00927404236573
3	0.19056483888763	-0.13644909765612	0.07046152309968
4	0.58422553883167	-0.21696226276259	0.13542356651691
5	0.58422553883167	0.33707999754362	-0.64578354990472
6	0.19056483888763	0.33707999754362	0.64578354990472
7	-0.04145457368920	-0.21696226276259	-0.13542356651691
8	-0.02692519074183	-0.13644909765612	-0.07046152309968
9	0.00069616789827	0.01098019299363	0.00927404236573
10	0	0.00549320005590	0.00549320005590
11	0	-0.00014203017443	-0.00014203017443

where

$$A(z)A(z^{-1}) = 0.5 + 0.5U(z),$$

$$B(z)B(z^{-1}) = 0.5 - 0.5U(z),$$

$$U(z)U(z^{-1}) = 1 - 2H_{0,0}(z)H_{0,0}(z^{-1}), M = N/2 - 1,$$

$$\text{and } H_{i,l}(z) = \sum_n h_i(2n - l)z^{-n} \text{ for } i, l = 0, 1.$$

3) *Filter Design*: First, obtain a lowpass filter, $h_0(n)$, which has an even-length and which satisfies the symmetric condition of Eq.(5). The design procedure is as follows:

- 1) Knowing $H_0(z)$ and, thus $H_{0,0}(z)$, use spectral factorization to find $U(z)$ from $1 - 2H_{0,0}(z)H_{0,0}(z^{-1})$.
- 2) Find $A(z)$ and $B(z)$ from $H_{0,0}(z)$ and $U(z)$ by using factorization and root selection.
- 3) Find $H_{1,0}(z)$ and $H_{1,1}(z)$ by using Eq.(11) and Eq.(12), respectively.
- 4) Find $H_1(z)$ and $H_2(z)$ by using $H_{1,0}(z)$, $H_{1,1}(z)$ and Eq.(7).
- 5) Obtain (anti)symmetric wavelets h_1 and h_2 by using Eq.(8) and Eq.(9).
- 4) *Example*: To obtain a lowpass filter, $h_0(n)$, with a minimal length, the researchers in [25] and [26] used a maximally

flat lowpass even-length FIR filter with the following transfer function:

$$F_{m,n}(z) = \left(\frac{1+z^{-1}}{2} \right) \left(\frac{z+2+z^{-1}}{4} \right)^m \sum_{k=0}^n \binom{m+k-0.5}{k} \left(\frac{-z+2-z^{-1}}{4} \right)^k.$$

Unfortunately, although the setting of $H_0(z) := F_{m,n}(z)$ gives an $H_0(z)$ that does not satisfy Eq.(5), we can use a linear combination of various $F_{m,n}(z)$ values to obtain a $H_0(z)$ filter that does satisfy Eq.(5). For example, if we use a setting of

$$H_0(z) = z^{-4} \sqrt{2} (\alpha F_{2,1}(z) + (1-\alpha) F_{3,1}(z)), \quad (13)$$

then, for special values of α , $H_0(z)$ satisfies Eq.(5).

Figure 2 shows the filters for $\alpha = 1.0720$. Figure 3 shows the resulting scaling function and wavelets. Table I lists the coefficients of the filters h_0 , h_1 and h_2 .

5) *Two-Dimensional Extension*: The 2-D extension can be obtained by alternating between rows and columns, as is usually done for typical DWTs. The corresponding filter bank, which is illustrated in Fig. 4, is iterated on the lowpass branch (the first branch).

III. FAST MULTIREOLUTION-BASED IMAGE FUSION WITH ADDITIVE WAVELET DECOMPOSITION

A. The FIHS Fusion Method

The IHS fusion method, which is widely used in image fusion to exploit the complementary nature of MS images, converts the RGB space of a color image into IHS color space. The intensity component in the IHS space is replaced by a high-resolution Pan image and then transformed back into the original RGB space together with the previous hue band and saturation band, resulting in an IHS fused image. The IHS fusion for each pixel can be formulated by the following procedure:

1)

$$\begin{bmatrix} I \\ v_1 \\ v_2 \end{bmatrix} = \begin{bmatrix} \frac{1}{3} & \frac{1}{3} & \frac{1}{3} \\ -\frac{\sqrt{2}}{6} & -\frac{\sqrt{2}}{6} & \frac{2\sqrt{2}}{6} \\ \frac{1}{\sqrt{2}} & \frac{1}{\sqrt{2}} & 0 \end{bmatrix} \begin{bmatrix} R \\ G \\ B \end{bmatrix}. \quad (14)$$

2) The intensity component, I, is replaced by the Pan image.

3)

$$\begin{aligned} \begin{bmatrix} F(R) \\ F(G) \\ F(B) \end{bmatrix} &= \begin{bmatrix} 1 & \frac{-1}{\sqrt{2}} & \frac{1}{\sqrt{2}} \\ 1 & \frac{-1}{\sqrt{2}} & \frac{1}{\sqrt{2}} \\ 1 & \frac{1}{\sqrt{2}} & 0 \end{bmatrix} \begin{bmatrix} \text{Pan} \\ v_1 \\ v_2 \end{bmatrix} \\ &= \begin{bmatrix} 1 & \frac{-1}{\sqrt{2}} & \frac{1}{\sqrt{2}} \\ 1 & \frac{-1}{\sqrt{2}} & \frac{1}{\sqrt{2}} \\ 1 & \frac{1}{\sqrt{2}} & 0 \end{bmatrix} \begin{bmatrix} I + (\text{Pan} - I) \\ v_1 \\ v_2 \end{bmatrix} \\ &= \begin{bmatrix} R + (\text{Pan} - I) \\ G + (\text{Pan} - I) \\ B + (\text{Pan} - I) \end{bmatrix}, \end{aligned} \quad (15)$$

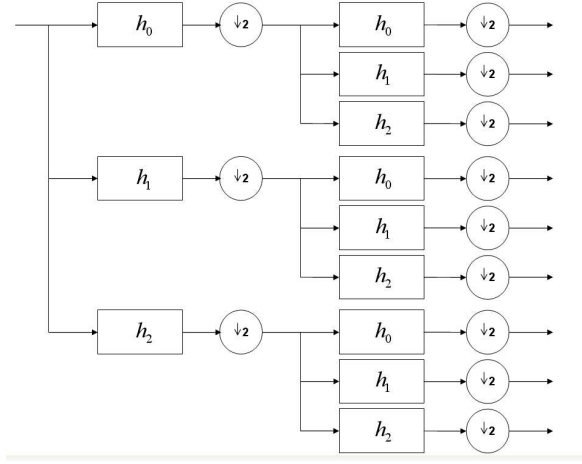


Fig. 4. An oversampled filterbank for a 2-D image

where $F(X)$ is the fused image of the X band, for $X = R, G,$ and B , respectively.

Equation (15) states that the fused image $[F(R), F(G), F(B)]^T$ can be easily obtained from the original image $[R, G, B]^T$ simply by using addition operations. That is, with this procedure, the IHS method can be implemented efficiently [18]. Aside from its fast computing capability for fusing images, this method can extend traditional three-order transformations to an arbitrary order.

The problem with the IHS-like fusion method is that spectral distortion may occur during the merging process. In Eq.(15), the large difference between the values of the Pan and the intensity images appears to cause the large spectral distortion of fused images. Indeed, the difference between the Pan and the intensity images causes the altered saturation component in the RGB-IHS conversion model [27].

B. The SWI Method Proposed by González-Audícana et al.

Recently, a SWI method proposed by González-Audícana et al. provided a solution based on the IHS method for image fusion. They used multiresolution wavelet decomposition to execute the detailed extraction phase, and they followed the IHS procedure to inject the spatial detail of the Pan image into the MS image. In other words, instead of using the Pan image in Eq. (15), they used the fusion results of the Pan image and the intensity image fused by the substitutive wavelet (SW) method. The fusion results of the Pan image and the intensity image are expressed as follows:

$$I_{\text{new}} = I_r + \sum_{k=1}^n W_{\text{Pan}_k}, \quad (16)$$

where I_r is the low-frequency version of the wavelet-transformed intensity image and $\sum_{k=1}^n W_{\text{Pan}_k}$ is the sum of high-frequency versions of the wavelet-transformed Pan image. Therefore, I_{new} contains the structural details of the Pan image's higher spatial resolution along with the rich spectral information of the MS images.

To apply any of the methods of image fusion described in this paper, the MS image and the Pan image must be accurately

superimposed. Thus, both images must be co-registered, and the MS image must be resampled to make its pixel size the same as the Pan image.

The steps for fusing images with the SWI method are as follows:

- 1) Apply the IHS transform to the RGB composition of the MS image. This transformation separates the spatial information of the MS image into the intensity component.
- 2) Generate a new Pan image, the histogram of which matches the histogram of the intensity image.
- 3) Apply the wavelet transform to the intensity image and to the histogram-matched Pan image. Because the spatial resolution ratio between the Pan image and the MS image is $2^n: 1$, an n -level wavelet decomposition must be performed.
- 4) Apply the inverse wavelet transform to the set composed of the low-frequency version of the wavelet-transformed intensity image and the sum of the high-frequency versions of the wavelet-transformed Pan image. This step adds the spatial details of the Pan image to the intensity image.
- 5) Apply the inverse IHS transform.

C. The FSWI Scheme

The proposed FSWI scheme involves the simple procedure based on the FIHS fusion method.

The general procedure is as follows:

- 1) Obtain an intensity image from MS images. In general, $I = (R + G + B)/3$.
- 2) Generate a new Pan image, the histogram of which matches the histogram of the intensity image.
- 3) Apply the wavelet transform to the difference image of the Pan image and the intensity image, that is, $\text{Pan} - I$, with n -level decomposition.
- 4) Fill the zeros in the low-frequency version of the wavelet-transformed difference image, and then perform the inverse wavelet transform.
- 5) Use simple addition operators to add the image obtained from steps 3) and 4) to each MS image.

In this general procedure, the choice of the intensity image is free but the choice of the n -level decomposition depends on the spatial resolution ratio of the Pan image and the MS image.

The FSWI scheme has a much simpler and faster approach than the SWI method. Moreover, theoretically, it is the exactly the same as the SWI method. Indeed, we show that the FSWI scheme is the same as the SWI method that is based on the FIHS fusion method.

Assume that, without the loss of generality, the SWI method is based on the FIHS fusion method instead of the standard IHS transform. This is because Eq. (15) holds. Moreover, as shown in the Appendix, when the value of Pan in Eq. (15) is replaced with the I_{new} value of Eq. (16), the following

equation is produced:

$$\begin{aligned}
 \begin{bmatrix} F(R) \\ F(G) \\ F(B) \end{bmatrix} &= \begin{bmatrix} R + (I_{\text{new}} - I) \\ G + (I_{\text{new}} - I) \\ B + (I_{\text{new}} - I) \end{bmatrix} \\
 &= \begin{bmatrix} R + (I_r + \sum_{k=1}^n W_{\text{Pan}_k} - I) \\ G + (I_r + \sum_{k=1}^n W_{\text{Pan}_k} - I) \\ B + (I_r + \sum_{k=1}^n W_{\text{Pan}_k} - I) \end{bmatrix} \\
 &= \begin{bmatrix} R + (\sum_{k=1}^n W_{\text{Pan}_k} - \sum_{k=1}^n W_{I_k}) \\ G + (\sum_{k=1}^n W_{\text{Pan}_k} - \sum_{k=1}^n W_{I_k}) \\ B + (\sum_{k=1}^n W_{\text{Pan}_k} - \sum_{k=1}^n W_{I_k}) \end{bmatrix} \\
 &= \begin{bmatrix} R + \sum_{k=1}^n W_{(\text{Pan}-I)_k} \\ G + \sum_{k=1}^n W_{(\text{Pan}-I)_k} \\ B + \sum_{k=1}^n W_{(\text{Pan}-I)_k} \end{bmatrix}
 \end{aligned} \tag{17}$$

where $\sum_{k=1}^n W_{I_k}$ is the sum of the high-frequency versions of the wavelet-transformed intensity image and $\sum_{k=1}^n W_{(\text{Pan}-I)_k}$ is the sum of the high-frequency versions of the wavelet-transformed difference image of the Pan image and the intensity image.

In addition, the idea of the FSWI scheme can be applied to the SW method. The SW method in [3] can be simplified with the following procedure:

$$\begin{aligned}
 \begin{bmatrix} F(R) \\ F(G) \\ F(B) \end{bmatrix} &= \begin{bmatrix} \sum_{k=1}^n W_{\text{Pan}_k} + R_r \\ \sum_{k=1}^n W_{\text{Pan}_k} + G_r \\ \sum_{k=1}^n W_{\text{Pan}_k} + B_r \end{bmatrix} \\
 &= \begin{bmatrix} \sum_{k=1}^n W_{\text{Pan}_k} + (R - \sum_{k=1}^n W_{R_k}) \\ \sum_{k=1}^n W_{\text{Pan}_k} + (G - \sum_{k=1}^n W_{G_k}) \\ \sum_{k=1}^n W_{\text{Pan}_k} + (B - \sum_{k=1}^n W_{B_k}) \end{bmatrix} \\
 &= \begin{bmatrix} R + (\sum_{k=1}^n W_{\text{Pan}_k} - \sum_{k=1}^n W_{R_k}) \\ G + (\sum_{k=1}^n W_{\text{Pan}_k} - \sum_{k=1}^n W_{G_k}) \\ B + (\sum_{k=1}^n W_{\text{Pan}_k} - \sum_{k=1}^n W_{B_k}) \end{bmatrix} \\
 &= \begin{bmatrix} R + \sum_{k=1}^n W_{(\text{Pan}-R)_k} \\ G + \sum_{k=1}^n W_{(\text{Pan}-G)_k} \\ B + \sum_{k=1}^n W_{(\text{Pan}-B)_k} \end{bmatrix}
 \end{aligned} \tag{18}$$

where $\sum_{k=1}^n W_{R_k}$, $\sum_{k=1}^n W_{G_k}$, and $\sum_{k=1}^n W_{B_k}$ are the sum of the high-frequency versions of the wavelet-transformed MS image, respectively, and $\sum_{k=1}^n W_{(\text{Pan}-R)_k}$, $\sum_{k=1}^n W_{(\text{Pan}-G)_k}$, and $\sum_{k=1}^n W_{(\text{Pan}-B)_k}$ are the sum of the high-frequency versions of the wavelet-transformed difference image of the Pan and the MS images, respectively.

The simply and fast procedure of the SW method is as follows:

- 1) Generate new Pan images, the histograms of which match the histograms of each band of the MS image.
- 2) Apply the wavelet transform to the difference image of the Pan image and the MS image, that is, $\text{Pan} - R$, $\text{Pan} - G$, and $\text{Pan} - B$, with n -level decomposition, respectively.
- 3) Fill the zeros in the low-frequency version of the wavelet-transformed difference images, and then perform the inverse wavelet transform, respectively.
- 4) Use simple addition operators to add images obtained from steps 2) and 3) to each MS image.

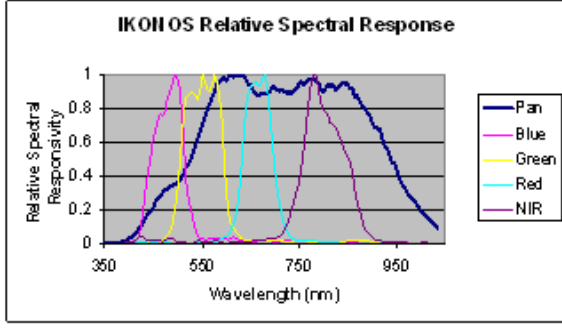


Fig. 5. Relative spectral responses of IKONOS image

D. The Spectral Distortion Problem for the IHS-like Method

As mentioned, a spectral distortion problem arises from the change of saturation during the fusion process. In an RGB-IHS conversion model, the saturation component (S) can be represented as follows:

$$S = 1 - \frac{3\min\{R, G, B\}}{R + G + B} = \frac{I - X_0}{I}, \quad (19)$$

where I is the intensity image and X_0 is the smallest value among R , G , and B for each pixel [27].

The new saturation value for the image fused by the FSWI method then becomes

$$\begin{aligned} S_{FSWI} &= 1 - \frac{3\min\{R + \delta, G + \delta, B + \delta\}}{R + G + B + 3\delta} \\ &= 1 - \frac{X_0 + \delta}{I + \delta} = \frac{I - X_0}{I + \delta}, \end{aligned} \quad (20)$$

where $\delta = \sum_{k=1}^n W_{(Pan-I)_k}$.

The relation between Eq.(19) and Eq.(20) is

$$\frac{S_{FSWI}}{S} = \frac{\frac{I - X_0}{I + \delta}}{\frac{I - X_0}{I}} = \frac{I}{I + \delta}. \quad (21)$$

This δ parameter is therefore a crucial factor in the spectral distortion problem when the value of δ is large. See [28] for more details.

E. IKONOS image fusion

When IHS-like fusion methods are used with IKONOS imagery, there is a significant color distortion, due primarily to the range of wavelengths in an IKONOS Pan image. Unlike the Pan images of SPOT and IRS sensors, IKONOS Pan images (as shown Fig. 5) have an extensive range of wavelengths—from visible to near-infrared (NIR). This difference obviously induces the color distortion problem in IHS fusion as a result of the mismatches; that is, the Pan image and the intensity image are spectrally dissimilar. In particular, the grey values of the Pan image in the green vegetated regions are far larger than the grey values of the intensity image because the areas covered by the vegetation are characterized by a relatively high reflectance of NIR and Pan bands as well as a low reflectance in the RGB bands. To minimize the radiance differences between the intensity image and the Pan image, Tu et al. included the NIR band in the definition of the intensity component [18].

The FIHS transform can be extended from three to four bands by

$$\begin{bmatrix} F(R) \\ F(G) \\ F(B) \\ F(NIR) \end{bmatrix} = \begin{bmatrix} R + \delta' \\ G + \delta' \\ B + \delta' \\ NIR + \delta' \end{bmatrix}, \quad (22)$$

where $\delta' = Pan - L$ and $L = (R + G + B + NIR)/4$. We call this method the eFIHS method. Indeed, compared with the IHS method, the eFIHS method provides much less the color distortions in fused images [18].

Similarly, the proposed FSWI method can be extended from three to four bands by

$$\begin{bmatrix} F(R) \\ F(G) \\ F(B) \\ F(NIR) \end{bmatrix} = \begin{bmatrix} R + \delta'' \\ G + \delta'' \\ B + \delta'' \\ NIR + \delta'' \end{bmatrix}, \quad (23)$$

where $\delta'' = \sum_{k=1}^n W_{(Pan-L)_k}$. We call it the eFSWI method.

Tu et al. [18] introduced eFIHS method with spectral adjustment applied to the intensity component, considering that

$$Pan - L' = Pan - \frac{R + a * G + b * B + NIR}{3}, \quad (24)$$

where a and b are weighting parameters defined to take into account that the spectral response of the Pan image does not cover that of the blue and green band. The value of these parameters was estimated experimentally after the fusion of 92 IKONOS images, covering different areas. According to the experimental results obtained by Tu et al., the best weighting parameters of a and b for G and B bands are 0.75 and 0.25, respectively. We call it the eFIHS-SA method.

Additionally, I propose the method of IKONOS image fusion based on the eFSWI and eFIHS-SA methods, which is as follows:

- 1) Obtain a new intensity image, $L' = (R + a * G + b * B + NIR)/3$.
- 2) Generate a new Pan image, the histogram of which matches the histogram of the new intensity image.
- 3) Apply the wavelet transform to the difference image of the Pan image and the new intensity image, that is, $Pan - L'$, with level two decomposition.
- 4) Fill the zeros in the low-frequency version of the wavelet-transformed difference image, and then perform the inverse wavelet transform.
- 5) Use simple addition operators to add the image obtained from steps 3) and 4) to each MS image.

We call this method the eFSWI-SA method.

IV. EXPERIMENTAL STUDY AND ANALYSIS

To merge an IKONOS Pan image and an MS image, an image of the Korean city of Daejeon, which was acquired on 9 March 2002, is used. The IKONOS imagery contains a 1 m Pan image and four-band 4 m MS images. The data for this experiment comprised a Pan image and four R , G , B , and NIR MS images.

A. The Factors for Quantitative Analysis

The quantitative analysis is based on the experimental results for the factors used in [28]–[31]: namely, the standard deviation (SD); the correlation coefficients (CCs); the relative average spectral error (RASE); the relative global dimensional synthesis error, which is known as *the erreur relative globale adimensionnelle de synthèse* (ERGAS); and the spatial quality measurement proposed by Zhou et al.

1) *The SD and the CCs*: The SD of the difference image in relation to the mean of the original image indicates the level of the error at any pixel. The lower the value of this parameter, the better the spectral quality of the fused image.

The CC between the original image and the fused image is defined as

$$CC(A, B) = \frac{\sum_{m,n}(A_{mn} - \bar{A})(B_{mn} - \bar{B})}{\sqrt{(\sum_{m,n}(A_{mn} - \bar{A})^2)(\sum_{m,n}(B_{mn} - \bar{B})^2)}}, \quad (25)$$

where \bar{A} and \bar{B} stand for the mean values of the corresponding data set, and CC is calculated globally for the entire image. The result of this equation shows similarity in the small structures between the original image and the fused image.

2) *The RASE and the ERGAS*: To estimate the global spectral quality of the fused images, we expressed the RASE index as a percentage [29], [30]. This percentage characterizes the average performance of the method of image fusion in the spectral bands considered. The RASE index is expressed as follows:

$$RASE = \frac{100}{M} \sqrt{\frac{1}{N} \sum_{i=1}^N RMSE^2(B_i)}, \quad (26)$$

where M is the mean radiance of the N spectral bands (B_i) of the original MS bands, and $RMSE$ is the root mean square error. The $RMSE$ value is as computed as follows:

$$RMSE^2(B_i) = bias^2(B_i) + SD^2(B_i). \quad (27)$$

The ERGAS index for the fusion is expressed as follows:

$$ERGAS = 100 \frac{h}{l} \sqrt{\frac{1}{N} \sum_{i=1}^N \frac{RMSE^2(B_i)}{M_i^2}}, \quad (28)$$

where h is the resolution of the high spatial resolution image, l is the resolution of the low spatial resolution image, and M_i is the mean radiance of each spectral band involved in the fusion. The lower the value of the RASE index and the ERGAS index, the higher the spectral quality of the fused images.

3) *Spatial quality measurement proposed by Zhou et al.*: To evaluate the detailed spatial information, a procedure proposed by Zhou et al. is used [31]. In this procedure, we filtered the Pan image and fused image with a Laplacian filter as follows:

$$\begin{pmatrix} -1 & -1 & -1 \\ -1 & 8 & -1 \\ -1 & -1 & -1 \end{pmatrix}. \quad (29)$$

The high correlation coefficients between the fused filtered image and the Pan filtered image (sCCs) indicate that most of the spatial information of the Pan image was incorporated

during the merging process. The sCC has the same definition as the CC.

B. Quantitative analysis

To assess the spectral and spatial quality of the fused images, spatially degraded Pan image and MS images were derived from the original images. For the experiment on the fusion of IKONOS images, the derived images had a resolution of 4 m and 16 m, respectively. These images were synthesized at a 4 m resolution and then compared to the original IKONOS MS images.

Using five estimators, Tables II shows the comparative analysis for IKONOS image fusion.

1) *Comparative analysis of the eFIHS method and the eFIHS-SA method of IKONOS image fusion*: In Table II, the images fused by the eFIHS method have lower spectral and spatial quality than images fused by the eFIHS-SA method. This difference is due to the non-ideal spectral responses of IKONOS imagery. Ideally, the RGB bands should fall just within the spectral range of the Pan band. In Fig. 5, the green and blue bands appear to overlap substantially, and the blue band mostly falls outside of the Pan band. Furthermore, the response of the Pan band is extended beyond the NIR band, thereby inducing the color distortion in IHS fusion. To cope with this problem, Tu et al. considered a simple spectral-adjusted scheme based on FIHS fusion. This scheme is very suitable for IKONOS image fusion, and the experimental results of Table II support this fact. Thus, in the IHS-like method, the precise choice of intensity component affects the performance of image fusion.

2) *Comparative analysis of the eFSWI method and the eFSWI-SA method of IKONOS image fusion*: The eFSWI method and the eFSWI-SA method are SW methods. The eFSWI method is based on the eFIHS method, and the eFSWI-SA method is based on the eFIHS-SA method. According to the above analysis, the eFSWI-SA method should perform much better than the eFSWI method. However, the eFSWI-SA method's values for the SD, CC, sCC, RASE and ERGAS are similar to the values of the eFSWI method for each DWT. The similarity of values means that the precise choice of the intensity component no longer affects the performance of image fusion in wavelet-based methods. One explanation for this phenomenon is that, unlike the eFIHS method and the eFIHS-SA method, the eFSWI method and the eFSWI-SA method inject MS images with detailed information extracted from the difference image of the Pan image and the new intensity image. That is, in wavelet-like methods, performance of image fusion is affected by the manner of extracting detailed information from a difference image (where detailed information refers to information that is not contained in the intensity image). Hence, the precise choice of DWT affects the performance of image fusion for wavelet-based methods.

3) *The possibility of using the introduced 2XDWT for image fusion*: Although the 2XDWT is not shift-invariant, it can be nearly shift-invariant. When the spacing between adjacent wavelets of the same scale is closer, the 2XDWT is less shift-sensitive than the DWT. In Table II, the sCC values of the

TABLE II
COMPARATIVE IKONOS FUSION RESULTS

		Initial	eFIHS	eFIHS-SA	eFSWI DWT	eFSWI 2XDWT	eFSWI ADWT	eFSWI-SA DWT	eFSWI-SA 2XDWT	eFSWI-SA ADWT
SD(%) (ideal value:0)	R	20.56	14.00	12.47	13.42	12.41	13.00	13.40	12.42	13.04
	G	19.19	14.76	13.42	13.24	12.38	12.67	13.18	12.32	12.67
	B	19.56	19.14	17.77	15.83	15.20	15.03	15.70	15.04	14.97
	NIR	22.99	14.46	12.93	12.88	11.61	12.52	12.93	11.73	12.62
\overline{SD}		20.57	15.59	14.14	13.84	12.90	13.30	13.80	12.87	13.32
CC (ideal value:1)	R	0.911	0.958	0.967	0.962	0.967	0.964	0.962	0.967	0.964
	G	0.925	0.955	0.963	0.964	0.968	0.967	0.964	0.969	0.967
	B	0.929	0.932	0.942	0.954	0.957	0.958	0.954	0.958	0.958
	NIR	0.846	0.939	0.951	0.951	0.960	0.954	0.951	0.960	0.953
\overline{CC}		0.902	0.946	0.955	0.957	0.963	0.960	0.957	0.963	0.960
sCC	R	0.284	0.998	0.998	0.991	0.997	0.995	0.992	0.998	0.995
	G	0.273	0.999	0.999	0.991	0.998	0.994	0.991	0.997	0.994
	B	0.257	0.998	0.997	0.989	0.996	0.993	0.989	0.996	0.992
	NIR	0.291	0.995	0.996	0.991	0.997	0.995	0.992	0.997	0.995
\overline{sCC}		0.276	0.998	0.998	0.990	0.997	0.994	0.991	0.997	0.994
RASE(%)		21.09	15.43	13.99	13.74	12.75	13.22	13.71	12.74	13.25
ERGAS		5.157	3.932	3.577	3.474	3.244	3.336	3.462	3.236	3.341

eFSWI 2XDWT and the eFSWI-SA 2XDWT are greater than the sCC values of the eFSWI DWT, the eFSWI-SA DWT, the eFSWI ADWT and the eFSWI-SA ADWT. In addition, the sCC values of the eFSWI 2XDWT and the eFSWI-SA 2XDWT are closer to the sCC values of the eFIHS method and the eFIHS-SA method than to the sCC values of other methods. This result confirms that 2XDWT produces a more satisfactory spatial resolution than other DWTs based on the eFSWI method and the eFSWI-SA method.

The values for the SD, RASE and ERGAS of the eFSWI 2XDWT and the eFSWI-SA 2XDWT are slightly lower than the corresponding values of the eFSWI DWT, the eFSWI-SA DWT, the eFSWI ADWT and the eFSWI-SA ADWT. In addition, the values for the CC of the eFSWI 2XDWT and the eFSWI-SA 2XDWT are slightly greater than the corresponding values of the eFSWI DWT, the eFSWI-SA DWT, the eFSWI ADWT and the eFSWI-SA ADWT. Hence, the spectral quality of images fused by the 2XDWT is slightly greater than the spectral quality of images fused by the DWT and ADWT based on the eFSWI and the eFSWI-SA methods.

In summary, the images fused by the 2XDWT have a more satisfactory spatial and spectral quality than those fused by the DWT and ADWT based on the eFSWI and the eFSWI-SA methods. Finally, the 2XDWT is a possible alternative to the two popular DWTs for image fusion.

4) *Comparative analysis of the proposed eFSWI-SA 2XDWT and other methods of IKONOS image fusion:* In Table II, the values for the bias, SD, RASE, and ERGAS of the eFSWI-SA 2XDWT method are all lower than the corresponding values of other methods, and the values of the CC are slightly greater. Hence, the spectral quality of images fused by the proposed eFSWI-SA 2XDWT method is much better than the spectral quality of images fused by other methods. In contrast, the sCC values of the eFSWI-SA

2XDWT method are similar to the sCC values of the eFIHS and the eFIHS-SA methods. The eFSWI-SA 2XDWT method consequently produces a satisfactory spatial resolution.

In summary, the author used five spectral and spatial estimators to analyze the spatial and spectral quality of the resulting images, and then compared the results with the quality of the fused images. The results show that the proposed eFSWI-SA 2XDWT method produces satisfactory quantitative results for IKONOS image fusion.

C. Visual analysis

Figure 6 shows the results of the visual fusion. In spite of the difficulty of determining which fusion method produces images with the best spatial and spectral quality, most fusion methods other than the DWT produce images of good spatial quality, and most fusion methods other than the eFIHS method produce images of good spectral quality. Even if only the 2XDWT is used to fuse images, some artifacts can be prevented from arising when the DWT is used.

V. CONCLUSION

A symmetric tight wavelet frame transform for image fusion that is based on additive wavelet decomposition have been presented. To validate this new approach, IKONOS Pan images and MS images were merged. To analyze the spatial and spectral quality of the resulting images, the following five factors were used: the bias, SD, CC, RASE, ERGAS, and sCC. And then the results with the quality of images fused by other methods of image fusion were compared. The values for the bias, SD, RASE, and ERGAS of the proposed eFSWI-SA 2XDWT method are all lower than the corresponding values of other wavelet-like methods, and the values of the CC are slightly greater. In addition, the sCC values of the eFSWI-SA 2XDWT method are similar to the sCC values of IHS-like

methods. The eFSWI 2XDWT method consequently produces a more satisfactory spectral and spatial resolution than other methods.

APPENDIX

In Eq.(18), we must show that

$$\sum_{k=1}^n W_{\text{Pan}_k} - \sum_{k=1}^n W_{I_k} = \sum_{k=1}^n W_{(\text{Pan-I})_k}.$$

We assume that, without the loss of generality, the *à trous* algorithm can be used as a DWT. Other DWTs can also be used for proof.

Given image P, we construct the sequence of approximations as follows:

$$\mathbb{C}(P) = P_1, \mathbb{C}(P_1) = \mathbb{C}^2(P) = P_2, \mathbb{C}(P_2) = \mathbb{C}^3(P) = P_3, \dots$$

To construct the sequence of approximations, the *à trous* algorithm performs successive convolutions with a filter obtained from an auxiliary function, named a scaling function. A B_3 cubic spline, which is generally used as the scaling function, leads to a convolution with a mask of 5×5 .

$$\frac{1}{256} \begin{pmatrix} 1 & 4 & 6 & 4 & 1 \\ 4 & 16 & 24 & 16 & 4 \\ 6 & 24 & 36 & 24 & 6 \\ 4 & 16 & 24 & 16 & 4 \\ 1 & 4 & 6 & 4 & 1 \end{pmatrix}.$$

That is,

$$\mathbb{C}^k(P) = P * \underbrace{B_3 * \dots * B_3}_k := P * B_3^k = P_k.$$

The wavelet planes are computed as the differences between two consecutive approximations: P_{k-1} and P_k . By letting $W_{P_k} = P_{k-1} - P_k$, $k = 1, \dots, n$, where $P_0 = P$, we can write the reconstruction formula as

$$P = P_r + \sum_{k=1}^n W_{P_k}$$

where P_r is a low-frequency version of P. We then have

$$\begin{aligned} & \sum_{k=1}^n W_{\text{Pan}_k} - \sum_{k=1}^n W_{I_k} \\ &= \sum_{k=1}^n (W_{\text{Pan}_k} - W_{I_k}) \\ &= \sum_{k=1}^n ((\text{Pan}_{k-1} - \text{Pan}_k) - (I_{k-1} - I_k)) \\ &= \sum_{k=1}^n ((\text{Pan}_{k-1} - I_{k-1}) - (\text{Pan}_k - I_k)) \\ &= \sum_{k=1}^n ((\text{Pan} * B_3^{k-1} - I * B_3^{k-1}) - (\text{Pan} * B_3^k - I * B_3^k)) \\ &= \sum_{k=1}^n ((\text{Pan-I}) * B_3^{k-1} - (\text{Pan-I}) * B_3^k) \end{aligned}$$

$$\begin{aligned} &= \sum_{k=1}^n ((\text{Pan-I})_{k-1} - (\text{Pan-I})_k) \\ &= \sum_{k=1}^n W_{(\text{Pan-I})_k}. \end{aligned}$$

ACKNOWLEDGMENT

The author would like to express their sincere gratitude to the anonymous referees for pointing out several typos and for some very helpful comments, and thank Dr. Kwanghoon Chi of the Korea Institute of Geoscience and Mineral Resources for providing the IKONOS images for this research.

REFERENCES

- [1] C. K. Munechika, J. S. Warnick, C. Salvaggio, and J. R. Schott, "Resolution Enhancement of Multispectral Image Data to Improve Classification Accuracy," *Photogrammetric Engineering and Remote Sensing*, vol. 59, no. 1, 1993, pp. 67-72.
- [2] Y. Zhang, "Understanding Image Fusion," *Photogrammetric Engineering and Remote Sensing*, vol. 70, no. 6, 2004, pp. 653-760.
- [3] J. Núñez, X. Otazu, O. Fors, A. Prades, V. Palà, and R. Arbiol, "Multiresolution-based image fusion with additive wavelet decomposition," *IEEE Transactions on Geoscience and Remote Sensing*, vol. 37, no. 3, 1999, pp. 1204-1211.
- [4] B. Aiazzi, L. Alparone, S. Baronti, and A. Garzelli, "Context-driven fusion of high spatial and spectral resolution data based on oversampled multiresolution analysis," *IEEE Transactions on Geoscience and Remote Sensing*, vol. 40, No. 10, 2002, pp. 2300-2312.
- [5] Y. Chibani and A. Houacine, "The joint use of IHS transform and redundant wavelet decomposition for fusing multispectral and panchromatic images," *International Journal of Remote Sensing*, vol. 23, no. 18, 2002, pp. 3821-3833.
- [6] Y. Chibani and A. Houacine, "Redundant versus orthogonal wavelet decomposition for multisensor image fusion," *Pattern Recognition*, vol. 36, 2003, pp. 879-887.
- [7] M. González-Audiciana, J. L. Saleta, R. G. Catalán, and R. García, "Fusion of Multispectral and Panchromatic Images Using Improved IHS and PCA Mergers Based on Wavelet Decomposition," *IEEE Transactions on Geoscience and Remote Sensing*, vol. 42, no. 6, 2004, pp. 1291-1299.
- [8] M. Choi, R. Y. Kim, M.-Y. Nam, and H. O. Kim, "Fusion of Multispectral and Panchromatic Satellite Images Using the Curvelet Transform," *IEEE Geoscience and Remote Sensing Letters*, vol. 2, no. 2, 2005, pp. 136-140.
- [9] M. González-Audiciana, X. Otazu, O. Fors, and A. Seco, "Comparison between Mallat's and the 'à trous' discrete wavelet transform based algorithms for the fusion of multispectral and panchromatic images," *International Journal of Remote Sensing*, vol. 26, no. 3, 2005, pp. 595-614.
- [10] I. Daubechies, "Ten Lectures on Wavelets," Philadelphia, PA: SIAM, 1992.
- [11] A. Ron and Z. W. Shen, "Affine systems in $L_2(\mathbb{R}^d)$: the analysis of the analysis operator," *Journal of Functional Analysis*, vol. 148, no. 2, 1997, pp. 408-447.
- [12] Z. Cvetković and M. Vetterli, "Oversampled filter banks," *IEEE Transactions on Signal Processing*, vol. 46, no. 5, 1998, pp. 1245-1255.
- [13] H. Bölcskei, F. Hlawatsch, and H. G. Feichtinger, "Frame-theoretical analysis of oversampled filter banks," *IEEE Transactions on Signal Processing*, vol. 46, no. 12, 1998, pp. 3256-3268.
- [14] C. K. Chui and W. He, "Compactly supported tight frames associated with refinable functions," *Applied and Computational Harmonic Analysis*, vol. 8, 2000, pp. 293-319.
- [15] C. K. Chui, W. He, and J. Stöckler, "Compactly supported tight and sibling frames with maximum vanishing moments," *Applied and Computational Harmonic Analysis*, vol. 13, 2002, pp. 224-262.
- [16] I. Daubechies, B. Han, A. Ron, and Z. W. Shen, "Framelets: MRA-based constructions of wavelet frames," *Applied and Computational Harmonic Analysis*, vol. 14, 2003, pp. 1-46.
- [17] A. F. Abdelnour and I. W. Selesnick, "Symmetric Nearly Shift-Invariant Tight Frame Wavelets," *IEEE Transactions on Signal Processing*, vol. 53, no. 1, 2005, pp. 231-239.

- [18] T.-M. Tu, P. S. Huang, C.-L. Hung, and C.-P. Chang, "A Fast Intensity-Hue-Saturation Fusion Technique With Spectral Adjustment for IKONOS Imagery," *IEEE Geoscience and Remote sensing letters*, vol. 1, no. 4, 2004, pp. 309-312.
- [19] S. G. Mallat, "A theory for multiresolution signal decomposition: the wavelet representation," *IEEE Transactions on Pattern Analysis and Machine Intelligence*, vol. 11, 1989, pp. 674-693.
- [20] P. Dutilleul, "An implementation of the 'algorithme à trous' to compute the wavelet transform," in *Wavelets: Time-Frequency Methods and Phase Space*, J. M. Combes, A. Grossman, and Ph. Tchamitchian, Eds. Berlin, Germany: Springer-Verlag, 1989, pp. 298-304.
- [21] I. W. Selesnick and A. F. Abdelnour, "Symmetric wavelet tight frames with two generators," *Applied and Computational Harmonic Analysis*, vol. 17, 2004, pp. 211-225.
- [22] S. Orantara, T. D. Tran, P. N. Heller, and T. Q. Nguyen, "Lattice structure for regular paraunitary linear-phase filterbanks and M -band orthogonal symmetric wavelets," *IEEE Transactions on Signal Processing*, vol. 49, no. 11, 2001, pp. 2659-2672.
- [23] Q. T. Jiang, "Parameterization of masks for tight affine frames with two symmetric/antisymmetric generators," *Advances in Computational Mathematics*, vol. 18, 2003, pp. 247-268.
- [24] A. Petukhov, "Symmetric framelets," *Constructive Approximation*, vol. 19, no. 2, 2003, pp. 309-328.
- [25] O. Herrmann, "Design of nonrecursive filters with linear phase," *Electronics Letters*, vol. 6, no. 11, 1970, pp. 328-329.
- [26] T. Cooklev and A. Nishihara, "Maximally flat FIR filters," in *Proceeding of IEEE International Symposium on Circuits and Systems (ISCAS)*, Chicago, vol. 1, 1993, pp. 96-99.
- [27] T.-M. Tu, S.-C. Su, H.-C. Shyn, and P. S. Huang, "A new look at IHS-like image fusion methods," *Information Fusion*, vol. 2, no. 3, 2001, pp. 177-186.
- [28] M. Choi, "A New Intensity-Hue-Saturation Fusion Approach to Image Fusion with a Tradeoff Parameter," *IEEE Transactions on Geoscience and Remote sensing*, vol. 44, no. 6, 2006, pp. 1672-1682.
- [29] L. Wald, T. Ranchin, and M. Mangolini, "Fusion of Satellite images of different spatial resolution: Assessing the quality of resulting images," *Photogrammetric Engineering and Remote Sensing*, vol. 63, no. 6, 1997, pp. 691-699.
- [30] T. Ranchin and L. Wald, "Fusion of High Spatial and Spectral Resolution images: The ARSIS Concept and Its Implementation," *Photogrammetric Engineering and Remote Sensing*, vol. 66, 2000, pp. 49-61.
- [31] J. Zhou, D. L. Civco, and J. A. Silander, "A wavelet transform method to merge Landsat TM and SPOT panchromatic data," *International Journal of Remote Sensing*, vol. 19, no. 4, 1998, pp. 743-757.
- [32] S. J. Sangwine and T. A. Ell, "Color image filters based on hypercomplex convolution," *IEE Proceedings - Vision, Image and Signal Processing*, vol. 147, no. 2, 2000, pp. 89-93.
- [33] I. L. Kantor and A. S. Solodnikov, "Hypercomplex Numbers, an Elementary Introduction to Algebras," New York: Springer-Verlag, 1989.
- [34] C. E. Moxey, S. J. Sangwine and T. A. Ell, "Hypercomplex correlation techniques for vector images," *IEEE Transactions on Signal Processing*, vol. 51, 2003, pp. 1941-1953.

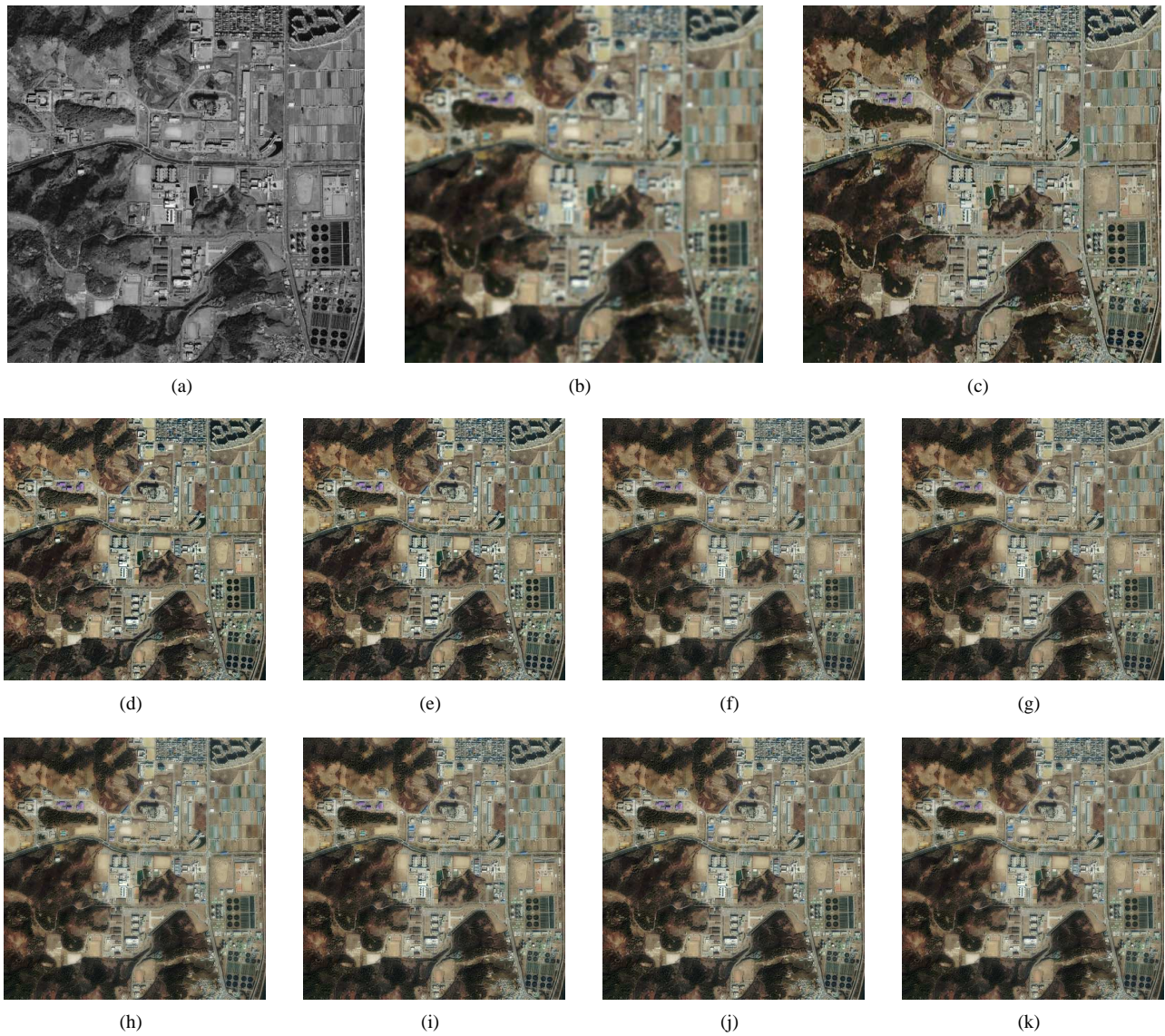


Fig. 6. (a) IKONOS Pan image; (b) degraded color image; (c) original IKONOS color image; (d) fused by the eFIHS; (e) fused by the eFIHS-SA; (f) fused by the eFSWI DWT; (g) fused by the eFSWI 2XDWT; (h) fused by the eFSWI ADWT; (i) fused by the eFSWI-SA DWT; (j) fused by the eFSWI-SA 2XDWT; (k) fused by the eFSWI-SA ADWT